COMPUTER METHODS IN MATERIALS SCIENCE

2021, vol. 21, no. 3, 139–148
https://doi.org/10.7494/cmms.2021.3.0753

Effective properties of periodic media in elastodynamic problems

Rolando Yera[1], Carlos G. Méndez[1], Pablo J. Sánchez[1,2], Alfredo E. Huespe[1,3*]

[1] CIMEC-UNL-CONICET, Predio Conicet Dr Alberto Cassano, CP 3000 Santa Fe, Argentina.
[2] Gimni UTN-FRSF, Lavaise 610, CP 3000 Santa Fe, Argentina.
[3] FIQ-UNL, Santiago del Estero 2800, CP 3000 Santa Fe, Argentina.

The authors of this paper would like to express their appreciation and honour to Prof. Maciej Pietrzyk. This paper is dedicated to him.

Abstract

This paper describes a homogenization model for evaluating the effective elastodynamic properties of acoustic metamaterials in problems involving wave propagation. The methodology is based on determining the constitutive equations in terms of averaged quantities observed at the macroscale. In this sense, the approach very closely follows the pioneering ideas introduced by Willis, and afterwards, followed by several authors in the last ten years. The distinctive characteristic of our approach is that we write the microscale equation in the spatial domain. The model is validated with previous results published in the literature, and our results replicate them almost exactly. The resulting homogenization model could be used as an additional tool for the topology design of acoustic metamaterials.

Keywords: effective properties of acoustic metamaterials, wave propagation in periodic media, Bloch waves, phononic crystals

1. Introduction

The construction of dispersion curves characterizing the response of acoustic metamaterials, or phononic crystals, displaying periodic micro-architectures subjected to wave propagation problems, is nowadays rather standard. There exists a consensus about how these curves have to be evaluated. Particularly, in layered composites, there are exact procedures and solutions available in the literature. Hussein et al. have studied this problem in several works and they have reported efficient numerical techniques to compute these dispersion curves (see the revision work of Huseein et al. (2014) and references cited therein, see also Krattiger and Hussein (2018)).

Alternatively, there is not a general agreement about how to evaluate the effective properties, observed at the macroscale level, of such acoustic metamaterials. This problem has been reported by several researchers, and many of the described models were derived from previous analyses coming from photonic crystals. We remark that the evaluation of the effective elasticity and density properties in an elastodynamic problem is the most typical case in metamaterials where

* Corresponding author: ahuespe@cimec.unl.edu.ar
ORCID ID: 0000-0001-7239-9805 (A.E. Huespe)

non-conventional situations can arise, as shown by Dong et al. (2017). For example, an interesting discussion about the attainment of non-conventional effective properties in heterogeneous materials with a microstructure is reported by Milton and Willis (2007). These authors discuss the consequences that such effective properties impose on the very fundamental responses of accelerating bodies in classical mechanics, in particular, the impact that they have on Newton's second law. A tensorial non-isotropic effective density, negative densities, or stiffnesses are typical results that can be obtained in these cases (double negative materials).

In this paper, we propose a numerical model to evaluate the effective properties of an acoustic metamaterial. These effective properties are obtained through an averaging procedure involving the constitutive response connecting the mechanical magnitudes observed at the macroscale as averaged quantities: stresses ($\boldsymbol{\Sigma}$), momentum density vector ($\boldsymbol{P}$), strains ($\boldsymbol{E}$), displacements ($\boldsymbol{U}$) and velocities ($\dot{\boldsymbol{U}}$), with those observed at the microscale: stresses ($\boldsymbol{\sigma}$), momentum density vector ($\boldsymbol{\rho}$), displacements ($\boldsymbol{u}$) and velocities ($\dot{\boldsymbol{u}}$). Our procedure follows closely the pioneering works of Willis (1997, 2012) to find the general form of constitutive relations in dynamic media with microstructure.

The original ideas of Willis were based on the ensemble averaging concept of a non-periodic composite, with these ideas then particularized for periodic materials. Nemat Nasser and co-authors have followed this line in several works. To cite only a few, we would mention Nemat-Nasser and Srivastava (2011) and Nemat-Nasser et al. (2011), and a good review is presented in the paper of Srivastava (2015). Nassar et al. (2016) also have followed the original ideas of Willis to implement a homogenization model in dynamic problems. Particularly relevant for the development of our present proposal is the paper by Nassar et al. (2015). The works of Willis, Nemat-Nasser et al., and Nassar et al. use the Green's function technique to solve the microscale problem arising from the mechanical formulation. They need to transform the mechanical variables to the Fourier or Laplace space. In our case, however, and as a distinctive characteristic, we formulate the microscale equations in the spatial domain that allows resolving pointwise eigenfields (displacements, stresses, etc.) with the conventional finite element method.

The effective properties obtained with the approach developed by Willis show a cross-coupling effect between the averaged stresses and momentums with the averaged strains and velocities. This result is also replicated by our model. Nevertheless, considering that these couplings have been widely studied in the literature, see the review of Willis (1997), we will not give any further details about this issue.

In our approach, we assume that the solutions of the elastodynamic wave propagation problem in periodic media are Bloch waves. An interesting description of Bloch waves in periodic media is found in the paper by Gazelet et al. (2013).

Several limitations of Willis' approach have been previously reported and the non-uniqueness of the solution was originally mentioned in the works of Willis. This author suggests including an additional eigenstrain in the constitutive equation of the average stress to recover uniqueness (see Nassar et al., 2015). Also, limitations of the model at high frequencies have been reported in Srivastava & Nemat-Nasser (2014). However, our primary interest in this work is to avoid the analysis of these issues. Such analysis is left for future work.

In the next section, we introduce a very short summary of the Bloch wave solutions for an elastodynamic problem in periodic media. We introduce the average field of a Bloch wave within a periodic micro-architecture. In Section 3, the homogenization model is introduced. The bridging scale equations, connecting both scales of analysis, are developed using a generalized version of the Hill–Mandel lemma. Section 4 presents the numerical treatment given to the microscale equation. We use a Lagrange Multiplier technique to relax the field constraint required by the homogenization model at the microscale. In Section 5 we describe some details of the numerical implementation of the homogenization algorithm. In Section 6, the methodology is numerically validated by comparing the results of the present model with those reported in the literature. Finally, the conclusions of this work are presented.

2. Theory

Let us consider the Bloch solution (Bloch type solutions are denoted by a superimposed hat) of a propagating wave in a periodic media with unit cell Ω_μ, $\hat{\varphi}(\boldsymbol{x})$, with (possible) complex wavenumber vector $\boldsymbol{k}$, which is also harmonic in time with frequency ω, whose expression is:

$$\hat{\varphi}(\boldsymbol{x}) = \varphi(\boldsymbol{x}) e^{i(\boldsymbol{k}\cdot\boldsymbol{x} - \omega t)} \tag{1}$$

This is typically a periodic function in space, $\varphi(\boldsymbol{x})$, modulated by a plane wave function $e^{i\boldsymbol{k}\cdot\boldsymbol{x}}$ and by the harmonic time function $e^{-i\omega t}$. The periodicity of $\varphi(\boldsymbol{x})$ is related to the unit cell of the periodic material Ω_μ. The function $\varphi(\boldsymbol{x})$ is identically repeated for every unit cell, and therefore, it satisfies the following identity: $\varphi(\boldsymbol{x}) = \varphi(\boldsymbol{x} + n_1\boldsymbol{a}_1 + n_2\boldsymbol{a}_2)$

where $\boldsymbol{a}_1$ and $\boldsymbol{a}_2$ are the primitive vectors of the Bravais lattice underlying of the periodic material (see Fig. 1), and n_1 and n_2 are arbitrary integer numbers.

Following the conventional treatment of harmonic problems in time, we replace the time derivative by the factor $-i\omega$ and remove the explicit time dependence $e^{-i\omega t}$ from the momentum balance equation, while only the spatial dependence is held explicit.

According to the ideas introduced originally by Willis, and particularly following the work of Nassar et al. (2015), we define the effective value of the mechanical terms.

Let us consider a particular term of the momentum balance equation, the divergence of the stress field. Using the Bloch wave expression for the stress:

$$\nabla_x \cdot \hat{\boldsymbol{\sigma}}(\boldsymbol{x}) = \nabla_x \cdot \boldsymbol{\sigma}(\boldsymbol{x}) e^{i\boldsymbol{k}\cdot\boldsymbol{x}} \tag{2}$$

we multiply this expression by $e^{i\boldsymbol{k}\cdot\boldsymbol{y}}$ (see Fig. 2) and replace the variable $\boldsymbol{X} = \boldsymbol{x} - \boldsymbol{y}$:

$$\nabla_x \cdot \boldsymbol{\sigma}(\boldsymbol{x}) e^{i\boldsymbol{k}\cdot(\boldsymbol{x}-\boldsymbol{y})} = \nabla_X \cdot \boldsymbol{\sigma}(\boldsymbol{X}+\boldsymbol{y}) e^{i\boldsymbol{k}\cdot\boldsymbol{X}} \tag{3}$$

Finally, we average this expression in the microcell Ω_μ, such as proposed in Nemat-Nasser and Srivastava (2011), to get:

$$\langle \nabla_X \cdot \boldsymbol{\sigma}(\boldsymbol{X}+\boldsymbol{y}) e^{i\boldsymbol{k}\cdot\boldsymbol{X}} \rangle_{\boldsymbol{y}\in\Omega_\mu} = \nabla_X \cdot \langle \boldsymbol{\sigma}(\boldsymbol{X}+\boldsymbol{y}) \rangle_{\boldsymbol{y}\in\Omega_\mu} e^{i\boldsymbol{k}\cdot\boldsymbol{X}} \tag{4}$$

where the notation $\langle(\cdot)\rangle$ means the average operator in Ω_μ. Following this concept, we define the average value of the generic field $\varphi(\boldsymbol{x})$ as follows:

$$\hat{\Phi}(\boldsymbol{X}) = \Phi(\boldsymbol{X}) e^{i\boldsymbol{k}\cdot\boldsymbol{X}} \tag{5}$$

where:

$$\Phi(\boldsymbol{X}) = \langle \varphi(\boldsymbol{X}+\boldsymbol{x}) \rangle_{\boldsymbol{y}\in\Omega_\mu} = \frac{1}{|\Omega_\mu|} \int_{\Omega_\mu} \varphi(\boldsymbol{X}+\boldsymbol{x}) d\boldsymbol{y} \tag{6}$$

There are three important issues which are remarked in the following items:

- Due to the periodicity of $\varphi(\boldsymbol{x})$, its average value $\langle \varphi(\boldsymbol{X}+\boldsymbol{y}) \rangle$ denoted $\Phi(\boldsymbol{X})$, is identical for every micro-cell Ω_μ at different positions $\boldsymbol{X}$. The macroscale coordinate $\boldsymbol{X}$ identifies the position of Ω_μ. Therefore, the effective value Φ does not depend on $\boldsymbol{X}$.
- The averaging procedure applied to all mechanical fields, preserves the form of the balance equation at the macroscale. These equations are derived below.
- In the following, we will not make a further distinction between the two variables $\boldsymbol{x}$ and $\boldsymbol{X}$. Additionally, it is understood that the domain where the average operation is performed is the microcell Ω_μ. In consequence, we remove the sub-index in the notation: $\langle\cdot\rangle_{\boldsymbol{y}\in\Omega_\mu}$.

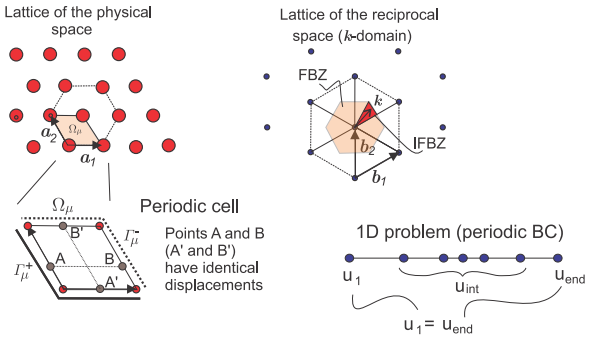

Fig. 1. Lattices of the physical and reciprocal spaces. Microcell Ω_μ with the boundaries Γ_μ^+ and Γ_μ^-. The points A and B (as well as A' and B') have identical displacements

The following identities hold for the symmetric gradient of a vector field $\hat{\varphi}$ and the corresponding average field $\hat{\Phi}(\boldsymbol{x})$:

$$\nabla_x \hat{\varphi}(\boldsymbol{x}) = \nabla_k(\varphi(\boldsymbol{x})) e^{i\boldsymbol{k}\cdot\boldsymbol{x}} \tag{7}$$

$$\nabla_k(\cdot) = \nabla_x(\cdot) + i\boldsymbol{k} \otimes^s (\cdot) \tag{8}$$

$$\nabla_x \hat{\Phi}(\boldsymbol{x}) = (\nabla_k \langle \varphi(\boldsymbol{x}) \rangle) e^{i\boldsymbol{k}\cdot\boldsymbol{x}} = i\boldsymbol{k} \otimes^s (\Phi) \tag{9}$$

where ∇_x is the symmetric gradient and $(\cdot \otimes^s \cdot)$ is the symmetric tensor product. The complex conjugate of the gradient is:

$$\overline{\nabla_k}(\cdot) = \overline{\nabla_x}(\cdot) - i\bar{\boldsymbol{k}} \otimes^s (\cdot) \tag{10}$$

3. Homogenization model

Let us consider the displacement and velocity fields as Bloch waves:

$$\hat{\boldsymbol{u}}(\boldsymbol{x}) = \boldsymbol{u}(\boldsymbol{x}) e^{i\boldsymbol{k}\cdot\boldsymbol{x}};\ \hat{\dot{\boldsymbol{u}}}(\boldsymbol{x}) = \dot{\boldsymbol{u}}(\boldsymbol{x}) e^{i\boldsymbol{k}\cdot\boldsymbol{x}} \tag{11}$$

where the periodic functions $\boldsymbol{u}(\boldsymbol{x})$ and $\dot{\boldsymbol{u}}(\boldsymbol{x})$, in Ω_μ, are approached as follows:

$$\boldsymbol{u}(\boldsymbol{y}) = \boldsymbol{U} + \tilde{\boldsymbol{u}}(\boldsymbol{y});\ \langle \boldsymbol{u} \rangle = \boldsymbol{U};\ \langle \tilde{\boldsymbol{u}} \rangle = 0 \tag{12}$$

$$\dot{\boldsymbol{u}}(\boldsymbol{y}) = \dot{\boldsymbol{U}} + \tilde{\dot{\boldsymbol{u}}}(\boldsymbol{y});\ \langle \dot{\boldsymbol{u}} \rangle = \dot{\boldsymbol{U}};\ \langle \tilde{\dot{\boldsymbol{u}}} \rangle = 0 \tag{13}$$

Considering item 1 of the previous section, we note that $\boldsymbol{U}$ does not depend on $\boldsymbol{X}$, and the macroscale displacement results: $\hat{\boldsymbol{U}}(\boldsymbol{X}) = \boldsymbol{U}(\boldsymbol{X}) e^{i\boldsymbol{k}\cdot\boldsymbol{x}}$.

The strain field in Ω_μ is:

$$\hat{\boldsymbol{\varepsilon}}(\boldsymbol{x}) = \boldsymbol{\varepsilon}(\boldsymbol{x}) e^{i(\boldsymbol{k}\cdot\boldsymbol{x}-\omega t)} \tag{14}$$

$$\boldsymbol{\varepsilon}(\boldsymbol{x}) = \nabla_k (\boldsymbol{U} + \tilde{\boldsymbol{u}}) = \underbrace{i\boldsymbol{k} \otimes^s \boldsymbol{U}}_{\boldsymbol{E}} + \nabla_k \tilde{\boldsymbol{u}} = \boldsymbol{E} + \nabla_k \tilde{\boldsymbol{u}} \tag{15}$$

Note that $\tilde{\boldsymbol{u}}$ is a periodic function with a null average value (see Equation (12)). Therefore, $\langle \nabla_k \tilde{\boldsymbol{u}} \rangle = \langle \nabla_x \tilde{\boldsymbol{u}} \rangle + i\boldsymbol{k} \otimes^s \langle \tilde{\boldsymbol{u}} \rangle = 0$, resulting:

$$\langle \boldsymbol{\varepsilon}(\boldsymbol{x}) \rangle = \boldsymbol{E} \tag{16}$$

3.1. A generalized version of the Hill–Mandel homogenization lemma

We assume that $\boldsymbol{U}$ and $\tilde{\boldsymbol{u}}$ can be arbitrarily defined with the condition that $\tilde{\boldsymbol{u}}$ is periodic and $\langle\tilde{\boldsymbol{u}}\rangle = 0$. Then, admissible variations of the average displacement $\boldsymbol{U}$ and displacement fluctuations $\tilde{\boldsymbol{u}}$ are defined as follows: $\delta\boldsymbol{U}$ is an arbitrary vector in $\mathbb{R}^{ndim}$, and $\delta\tilde{\boldsymbol{u}} \in V_u$, where the vector space V_u is defined as follows:

$$V_u = \{\delta\tilde{\boldsymbol{u}} \mid \delta\tilde{\boldsymbol{u}} \text{ is periodic; and } \langle\delta\tilde{\boldsymbol{u}}\rangle = 0\} \tag{17}$$

Admissible variations of the average strain are $\delta\boldsymbol{E} = i\boldsymbol{k} \otimes^s \delta\boldsymbol{U}$ and admissible strains in Ω_μ are: $\delta\boldsymbol{\varepsilon} = i\boldsymbol{k} \otimes^s \delta\boldsymbol{U} + \nabla_k(\delta\tilde{\boldsymbol{u}})$.

The Hill–Mandel homogenization principle is presented as follows:

$$\boldsymbol{\Sigma}: \overline{\delta\boldsymbol{E}} - i\omega\boldsymbol{P}\cdot\overline{\delta\boldsymbol{U}} = \langle\boldsymbol{\sigma}: \overline{\delta\boldsymbol{\varepsilon}} - i\omega\boldsymbol{p}\cdot\overline{\delta\tilde{\boldsymbol{u}}}\rangle \quad \forall\ \overline{\delta\boldsymbol{U}} \in \mathbb{R}^{ndim};\ \forall\ \overline{\delta\tilde{\boldsymbol{u}}} \in V_u \tag{18}$$

The symbols (:) and (·) denote internal products of second-order tensors and vectors, respectively. Also, the symbol $\overline{(\cdot)}$ represents the complex conjugate term[1].

In Equation (18), the expressions $\boldsymbol{\Sigma}$ and $\boldsymbol{P}$ are averaged variables conjugate to $\boldsymbol{E}$ and $\dot{\boldsymbol{U}}$, respectively. Arbitrary variations of $\boldsymbol{U}$ and $\tilde{\boldsymbol{u}}$ define the connection of $\boldsymbol{\Sigma}$ and $\boldsymbol{P}$ with the microscale (non-averaged) variables, as shown in the following:

– Performing arbitrary variations of $\delta\boldsymbol{U}$, expression (18) gives:

$$i\boldsymbol{k}\boldsymbol{\Sigma} + i\omega\boldsymbol{P} = \langle i\boldsymbol{k}\boldsymbol{\sigma} - i\omega\boldsymbol{p}\rangle \tag{19}$$

Considering each term separately, and given that this expression has to be satisfied for different values of $\boldsymbol{k}$ and ω^2, then, the Equation (19) is satisfied if:

$$\boldsymbol{\Sigma} = \langle\boldsymbol{\sigma}\rangle \text{ and } \boldsymbol{P} = \langle\boldsymbol{p}\rangle \tag{20}$$

– Performing arbitrary variations of $\delta\tilde{\boldsymbol{u}}$, expression (18) gives:

$$\langle\boldsymbol{\sigma}: \overline{\nabla_k\delta\tilde{\boldsymbol{u}}} - i\omega\boldsymbol{p}\cdot\overline{\delta\tilde{\boldsymbol{u}}}\rangle = 0;\ \forall\ \overline{\delta\tilde{\boldsymbol{u}}} \in V_u \tag{21}$$

4. The Lagrange Multiplier approach

In (21), to relieve the null average value constraint characterizing the functions in V_u and following Roca et al. (2019), we introduce a Lagrange Multiplier approach. In this case, Equation (21) can be rewritten as follows:

$$\langle\boldsymbol{\sigma}: \overline{\nabla_k\delta\tilde{\boldsymbol{u}}} - i\omega\boldsymbol{p}\cdot\overline{\delta\tilde{\boldsymbol{u}}}\rangle - \boldsymbol{\lambda}\cdot\langle\delta\tilde{\boldsymbol{u}}\rangle = 0;\ \forall\ \delta\tilde{\boldsymbol{u}} \text{ periodic} \tag{22}$$

$$-\langle\delta\tilde{\boldsymbol{u}}\rangle\cdot\delta\boldsymbol{\lambda} = 0;\ \ \forall\ \delta\boldsymbol{\lambda} \in \mathbb{R}^{ndim} \tag{23}$$

where $\boldsymbol{\lambda} \in \mathbb{R}^{ndim}$ is the Lagrange Multiplier. In this formulation, the variations $\delta\tilde{\boldsymbol{u}}$ are not constrained to have a null average.

Taking the variational Equation (22), and particularizing the variational displacement $\delta\tilde{\boldsymbol{u}}$ to be an arbitrary uniform vector $\boldsymbol{a} \in \mathbb{R}^{ndim}$, result:

$$\langle i\boldsymbol{k}\boldsymbol{\sigma} + i\omega\boldsymbol{p}\rangle = -\boldsymbol{\lambda} \tag{24}$$

which, jointly with Equation (19), provides a balance equation of averaged terms:

$$i\boldsymbol{k}\boldsymbol{\Sigma} + i\omega\boldsymbol{P} + \boldsymbol{\lambda} = -\overline{\nabla_k}\,\boldsymbol{\Sigma} + i\omega\boldsymbol{P} + \boldsymbol{\lambda} = 0 \tag{25}$$

The intermediate identity arises after considering that $\boldsymbol{\Sigma}$ does not depend on $\boldsymbol{x}$.

5. Microcell problem

Let the constitutive equation be given in terms of the periodic functions as follows:

$$\boldsymbol{\sigma} = \mathbb{C}\nabla_k\boldsymbol{u} = \mathbb{C}(\boldsymbol{E} + \nabla_k\tilde{\boldsymbol{u}}) \tag{26}$$

$$\boldsymbol{p} = \rho\dot{\boldsymbol{u}} = \rho(\dot{\boldsymbol{U}} + \dot{\tilde{\boldsymbol{u}}}) \tag{27}$$

where $\mathbb{C}$ is the elasticity tensor and ρ the density. Replacing both expressions in (22) and (23), result:

$$\langle\mathbb{C}\nabla_k\tilde{\boldsymbol{u}}: \overline{\nabla_k\delta\tilde{\boldsymbol{u}}} - \omega^2\rho\tilde{\boldsymbol{u}}\cdot\overline{\delta\tilde{\boldsymbol{u}}}\rangle - \boldsymbol{\lambda}\cdot\langle\delta\tilde{\boldsymbol{u}}\rangle = -\langle\mathbb{C}\boldsymbol{E}: \overline{\nabla_k\delta\tilde{\boldsymbol{u}}} - i\omega\rho\dot{\boldsymbol{U}}\cdot\ \overline{\delta\tilde{\boldsymbol{u}}}\rangle \tag{28}$$

$$-\langle\delta\tilde{\boldsymbol{u}}\rangle\cdot\delta\boldsymbol{\lambda} = 0 \tag{29}$$

$$\forall\ \delta\tilde{\boldsymbol{u}} \text{ periodic};\ \forall\ \delta\boldsymbol{\lambda} \in \mathbb{R}^{ndim}$$

5.1. Numerical implementation

The displacements $\tilde{\boldsymbol{u}}$ in Ω_μ are interpolated through a conventional FE approach:

$$\tilde{\boldsymbol{u}}(\boldsymbol{y}) = \boldsymbol{N}(\boldsymbol{y})[\tilde{\boldsymbol{u}}] \tag{30}$$

$$\nabla_k\tilde{\boldsymbol{u}} = \boldsymbol{B}[\tilde{\boldsymbol{u}}] + i\boldsymbol{k} \otimes^s \boldsymbol{N}[\tilde{\boldsymbol{u}}] = \boldsymbol{B}_k[\tilde{\boldsymbol{u}}] \tag{31}$$

where $\boldsymbol{N}$ is the matrix of shape functions and $[\tilde{\boldsymbol{u}}] \in \mathbb{R}^{ndof}$ is the vector gathering the full nodal displacement set of the finite element mesh. The total number of Degrees of Freedom (DOFs) is denoted *ndof*. The matrix $\boldsymbol{B}$ is the conventional finite element strain-displacement matrix. Also, for notation consistency, we call $[\lambda] \in \mathbb{R}^{ndim}$ the Lagrange Multiplier vector.

[1] Note that by adopting admissible displacement variations, $\delta\tilde{\boldsymbol{u}}$, which have a Bloch-wave form with conjugate admissible displacements given by $\overline{\delta\tilde{\boldsymbol{u}}} = \delta\boldsymbol{u}e^{-i\boldsymbol{k}\cdot\boldsymbol{x}}$, then, the virtual internal work results: $\hat{\boldsymbol{\sigma}}:\nabla_x\overline{\delta\tilde{\boldsymbol{u}}} = \hat{\boldsymbol{\sigma}}: \overline{\nabla_k\delta\tilde{\boldsymbol{u}}}$ Thus, this internal product can be written only in terms of the periodic parts of $\hat{\boldsymbol{\sigma}}$ and $\delta\hat{\boldsymbol{\sigma}}$. This property is used in all the internal products reported in this paper.

[2] The wavenumber $\boldsymbol{k}$ and frequency ω are not arbitrary. They have to be consistent with the dispersion curves of the material.

Introducing this approach into equations (28) and (29), results in the following discrete equation system:

$$\begin{bmatrix} \mathbb{K}_{dyn} & -\langle \boldsymbol{N} \rangle^T \\ -\langle \boldsymbol{N} \rangle & 0 \end{bmatrix} \begin{bmatrix} [\tilde{\boldsymbol{u}}] \\ [\lambda] \end{bmatrix} = \begin{bmatrix} -\langle \overline{\boldsymbol{B}_k}^T \mathbb{C} \boldsymbol{E} - i\omega\rho \boldsymbol{N}^T \dot{\boldsymbol{U}} \rangle \\ \boldsymbol{0} \end{bmatrix} \quad (32)$$

where $\mathbb{K}_{dyn} = (\mathbb{K}(\boldsymbol{k}) - \omega^2 \mathbb{M})$ is the sum of an averaged stiffness matrix $\mathbb{K}(\boldsymbol{k}) = \langle \overline{\boldsymbol{B}_k}^T \mathbb{C} \boldsymbol{B}_k \rangle$ and an averaged mass matrix $\mathbb{M} = \langle \rho \boldsymbol{N}^T \boldsymbol{N} \rangle$.

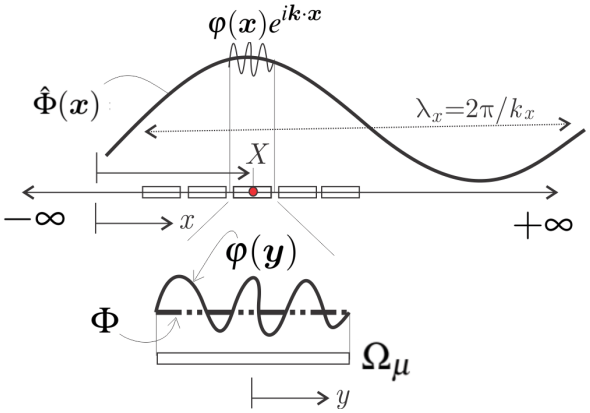

Fig. 2. Schematic description of the Bloch wave solution $\hat{\varphi}(\boldsymbol{x})$ for a periodic material and its average field $\hat{\Phi}(\boldsymbol{x})$

The periodicity of the field $\tilde{\boldsymbol{u}}$ requires that the nodal values of $[\tilde{\boldsymbol{u}}]$ on the boundary Γ_μ^-, of Ω_μ, are identical to those of the nodes on the boundary Γ_μ^+. This restriction is imposed via the following expression:

$$[\tilde{\boldsymbol{u}}] = \mathbb{P}[\tilde{\boldsymbol{u}}]_r \quad (33)$$

where $[\tilde{\boldsymbol{u}}]_r$ is the vector gathering the displacement DOFs of the interior nodes of Ω_μ plus the nodes on the boundary Γ_μ^+ of Ω_μ, see Figure 1. For a one-dimensional (1-D) system, Equation (33) is written as follows:

$$[\tilde{\boldsymbol{u}}] = \begin{bmatrix} u_1 \\ \boldsymbol{u}_{\text{int}} \\ u_{end} \end{bmatrix} = \mathbb{P}[\tilde{\boldsymbol{u}}]_r = \begin{bmatrix} 1 & \boldsymbol{0} \\ 0 & \boldsymbol{1} \\ 1 & \boldsymbol{0} \end{bmatrix} \begin{bmatrix} u_1 \\ \boldsymbol{u}_{\text{int}} \end{bmatrix} \quad (34)$$

where, as schematized in Figure 1, the u_1 DOF is on the boundary Γ_μ^+, u_{end} is the DOF on the boundary Γ_μ^- and $\boldsymbol{u}_{int}$ are the full set of interior DOFs.

Using the reduced DOFs, equation system (32) is rewritten as follows:

$$\underbrace{\begin{bmatrix} \mathbb{P}^T \mathbb{K}_{dyn} \mathbb{P} & -\mathbb{P}^T \langle \boldsymbol{N} \rangle^T \\ -\langle \boldsymbol{N} \rangle \mathbb{P} & \boldsymbol{0} \end{bmatrix}}_{\mathbb{D}} \begin{bmatrix} [\tilde{\boldsymbol{u}}]_r \\ [\lambda] \end{bmatrix} = \begin{bmatrix} -\mathbb{P}^T \langle \overline{\boldsymbol{B}_k}^T \mathbb{C} \boldsymbol{E} - i\omega\rho \boldsymbol{N}^T \dot{\boldsymbol{U}} \rangle \\ \boldsymbol{0} \end{bmatrix} \quad (35)$$

Thus:

$$\begin{bmatrix} [\tilde{\boldsymbol{u}}] \\ [\lambda] \end{bmatrix} = \begin{bmatrix} \mathbb{F} & \mathbb{A} \\ \mathbb{G} & \mathbb{I} \end{bmatrix} \begin{bmatrix} \boldsymbol{E} \\ \dot{\boldsymbol{U}} \end{bmatrix} \quad (36)$$

where:

$$\mathbb{A} = -\overbrace{\mathbb{P}(\mathbb{D}^{-1})_{11}\mathbb{P}^T}^{\mathbb{Q}} \langle \overline{\boldsymbol{B}_k}^T \mathbb{C} \rangle = -\mathbb{Q} \langle \overline{\boldsymbol{B}_k}^T \mathbb{C} \rangle \quad (37)$$

$$\mathbb{F} = +i\omega \mathbb{Q} \langle \rho \boldsymbol{N}^T \rangle \quad (38)$$

$$\mathbb{G} = -(\mathbb{D}^{-1})_{21} \mathbb{P}^T \langle \overline{\boldsymbol{B}_k}^T \mathbb{C} \rangle \quad (39)$$

$$\mathbb{I} = +i\omega (\mathbb{D}^{-1})_{21} \mathbb{P}^T \langle \rho \boldsymbol{N}^T \rangle \quad (40)$$

where $(\mathbb{D}^{-1})_{11}$ and $(\mathbb{D}^{-1})_{21}$ are the corresponding sub-blocks of the inverse matrix $(\mathbb{D}^{-1})$ which multiply the non-null right-hand side of (35) to provide $[\tilde{\boldsymbol{u}}]$ and $[\lambda]$, respectively.

The expressions (36) are replaced in equations (26) and (27); and the resulting stress and momentum terms are finally replaced into Equation (20), giving:

$$\begin{bmatrix} \boldsymbol{\Sigma} \\ \boldsymbol{P} \end{bmatrix} = \begin{bmatrix} \langle \mathbb{C}(\boldsymbol{E} + \boldsymbol{B}_k[\tilde{\boldsymbol{u}}]) \rangle \\ \langle \rho(\dot{\boldsymbol{U}} - i\omega \boldsymbol{N}[\tilde{\boldsymbol{u}}]) \rangle \end{bmatrix} = \begin{bmatrix} \mathbb{C}^* & \mathbb{S}_1 \\ \mathbb{S}_2 & \boldsymbol{\rho}^* \end{bmatrix} \begin{bmatrix} \boldsymbol{E} \\ \dot{\boldsymbol{U}} \end{bmatrix} \quad (41)$$

where the matrices $\mathbb{C}^*$, $\mathbb{S}$ and $\boldsymbol{\rho}^*$ are:

$$\mathbb{C}^* = \langle \mathbb{C} \rangle + \langle \mathbb{C} \boldsymbol{B}_k \rangle \mathbb{A} = \langle \mathbb{C} \rangle - \langle \mathbb{C} \boldsymbol{B}_k \rangle \mathbb{Q} \langle \overline{\boldsymbol{B}_k}^T \mathbb{C} \rangle \quad (42)$$

$$\mathbb{S}_1 = \langle \mathbb{C} \boldsymbol{B}_k \rangle \mathbb{F} = i\omega \langle \mathbb{C} \boldsymbol{B}_k \rangle \mathbb{Q} \langle \rho \boldsymbol{N}^T \rangle \quad (43)$$

$$\mathbb{S}_2 = i\omega \langle \rho \boldsymbol{N} \rangle \mathbb{Q} \langle \overline{\boldsymbol{B}_k}^T \mathbb{C} \rangle \quad (44)$$

$$\boldsymbol{\rho}^* = \langle \rho \rangle \boldsymbol{1} - i\omega \langle \rho \boldsymbol{N} \rangle \mathbb{F} = \langle \rho \rangle \boldsymbol{1} + \omega^2 \langle \rho \boldsymbol{N} \rangle \mathbb{Q} \langle \rho \boldsymbol{N}^T \rangle \quad (45)$$

Note that $\mathbb{D}$ is a Hermitian matrix, as well as it's inverse $\mathbb{D}^{-1}$ and the sub-matrix $(\mathbb{D}^{-1})_{11}$. Therefore, the matrix $\mathbb{Q}$ is also a Hermitian matrix, which determines real matrices $\mathbb{C}^*$ and $\boldsymbol{\rho}^*$.

5.2. Dispersion curves

We observe in the present model that the average balance Equation (25) jointly with the microcell Equation (21) result equivalent to solve the microcell variational problem (21) with admissible displacement variations $\delta\tilde{\boldsymbol{u}}$ being not necessarily spatial functions with null average. Thus, these equations can be similarly written as follows:

$$\langle \boldsymbol{\sigma}(\boldsymbol{u}) : \overline{\nabla_k \delta \boldsymbol{u}} - i\omega \boldsymbol{p}(\dot{\boldsymbol{u}}) \cdot \overline{\delta \boldsymbol{u}} \rangle = 0; \ \forall \ \delta\tilde{\boldsymbol{u}} \text{ periodic} \quad (46)$$

and the discrete problem is:

$$\mathbb{P}^T \mathbb{K}_{dyn} \mathbb{P}[\boldsymbol{u}]_r = [\mathbb{P}^T (\mathbb{K}(\boldsymbol{k}) - \omega^2 \mathbb{M}) \mathbb{P}][\boldsymbol{u}]_r = \boldsymbol{0} \quad (47)$$

The solution of this eigenvalue problem provides the dispersion curves of the periodic material.

It is important to remark that even when the matrix $\mathbb{P}^T\mathbb{K}_{dyn}\mathbb{P}$ is singular for every pair $(\omega - \boldsymbol{k})$ lying on the dispersion curves, the matrix $\mathbb{D}$ in Equation (35) is not singular for these pairs, and therefore, it can be inverted. A good condition number of this matrix $\mathbb{D}$ requires that the column vectors $-\mathbb{P}^T\langle \boldsymbol{N}\rangle^T$ and the row vector $-\langle \boldsymbol{N}\rangle\mathbb{P}$ be scaled. We suggest multiplying both vectors by the scalar factor $\alpha = \omega^2\langle\rho\rangle$.

6. Numerical assessment of the homogenization model

In this section, we validate the homogenization model. First, we solve two 1-D wave propagation problems with symmetric and non-symmetric multilayer configurations (sub-Sections 6.1 and 6.2, respectively). The obtained solutions are compared with reported results.

In the last sub-Section, we solve a two-dimensional (2-D) problem whose band structure has also been reported in several works. Therefore, these results allow us to validate the computation of dispersion diagrams in 2-D cases. The homogenized properties obtained with our model are finally plotted.

6.1. Effective properties of one symmetric layered composite

We evaluate the effective properties of the layered composite whose unit cell is depicted in Figure 3a. It consists of a heavy and stiff layer (Layer 3) placed between two soft and light layers (Layers 2). These layers are embedded into a pair of stiffer layers (Layers 1). The effective properties of this composite have been reported by Nemat-Nasser and Srivastava (2011). The objective that we pursue in this case is to validate our model by comparing our results with those reported in Nemat-Nasser and Srivastava (2011)[3].

The first two modes of the dispersion curves are shown in Figure 3b. Figure 3c depicts the effective compliance ($1/C^{eff}$), which is computed by following to Nemat-Nasser and Srivastava (2011):

$$C^{eff} = \mathbb{C}^* - \frac{\omega}{k}\,\mathbb{S}_1 \tag{48}$$

This identity is derived by assuming 1-D conditions, as well as, that[4] $\dot{U} = -(i\omega)E/(ik)$, which is replaced in the first Equation (41). Identically, in the second Equation (41), the term E is replaced by $E = -(ik)\dot{U}/(i\omega)$ to obtain the effective density:

$$\rho^{eff} = \boldsymbol{\rho}^* - \frac{k}{\omega}\,\mathbb{S}_2 \tag{49}$$

that is depicted in Figure 3d.

These results have been plotted for different FE mesh refinement. Three curves are plots for Nelem = 5, Nelem = 15, and Nelem = 21 (Nelem: number of finite elements used to discretize the microcell). The finite elements in the case of Nelem = 21 are distributed as follows: 6 elements for each Layer 1, 3 for each Layer 2, and 3 for Layer 3. In the remaining cases, the number of finite elements is uniformly distributed in the layer domains.

In Figure 3d, effective density vs. frequency plot, we copy the results taken from the reference work. Note the good agreement between both solutions.

6.2. Effective properties of one asymmetric layered composite

For asymmetric unit cells (i.e., when the phases are not disposed in a symmetrical spatial pattern), the out-of-diagonal terms ($\mathbb{S}_1$, $\mathbb{S}_2$) in the matrix on the right-hand side of Equation (41) are complex-valued and introduce the fully coupling complex-relationship between ($\boldsymbol{E}$, $\dot{\boldsymbol{U}}$) and ($\boldsymbol{\Sigma}$, $\boldsymbol{P}$).

Following Nemat-Nasser and Srivastava (2011), we present the results of the unit cell displayed in Figure 4a. Note that the material parameters are similar to the previous multilayer case, however, the thicknesses of the Layers 2 are dissimilar, introducing a non-symmetrical distribution of layer thicknesses.

The following results have been obtained with a finite element mesh of 21 finite elements (6 elements for each Layer 1, 3 for each Layer 2, and 3 for Layer 3).

Figure 4b displays the dispersion curves of the first two modes. Figure 4c displays the effective compliance ($1/\mathbb{C}^*$), which is comparable to the plots reported by the reference work. Also, to compare the results of the reference work we plot in Figure 4d and Figure 4e the out-of diagonal terms ($-\mathbb{S}_1/\mathbb{C}^*$) and ($\mathbb{S}_2/\mathbb{C}^*$), respectively. As can be noted, our results compare very well with those of the reference work.

[3] The approach adopted in Nemat-Nasser and Srivastava (2011) to evaluate the effective properties consists on formulating the microscale problem through a pair of integral equations involving the eigenfields $\boldsymbol{\sigma}$ and $\boldsymbol{u}^*$. Then, instead of seeking a point-wise solution of these field, as we do, they calculate their volume averages in terms of the average stress and velocity: $\boldsymbol{\Sigma}$ and $\dot{\boldsymbol{U}}$.

[4] The identity $-i\omega E = ik\dot{U}$ results from the kinematical relation at the macroscale (averaged variables): $\hat{\boldsymbol{E}} = \nabla_x\hat{\boldsymbol{U}}$.

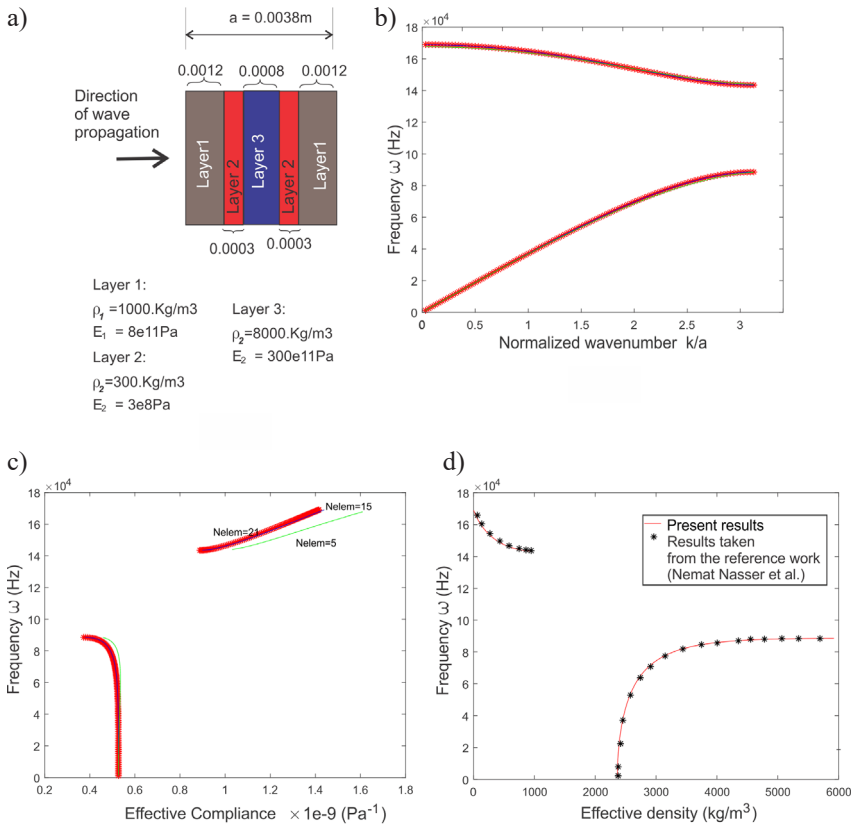

Fig. 3. Effective properties of one symmetric layered composite: a) configuration of the composite multilayer and the wave propagation problem; b) dispersion curves of the first two modes; c) effective compliance; d) effective density

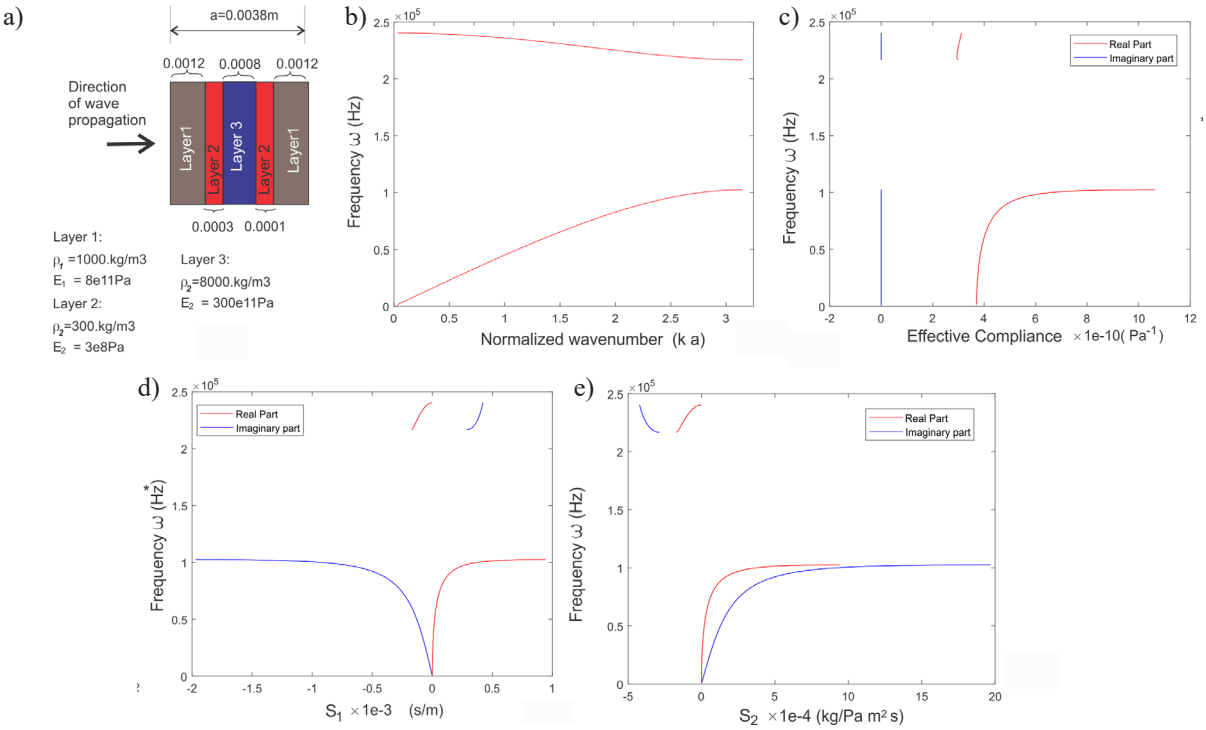

Fig. 4. Effective properties of an asymmetric layered composite obtained with (Nelem = 21): a) schematic diagram of the composite multilayer and the wave propagation problem; b) dispersion curves of the first two modes; c) effective compliance; d) S_1 component of the effective constitutive matrix; e) S_2 component of the effective constitutive matrix

6.3. Composite with square scatterers

We analyze a wave propagation problem in a composite medium with a homogeneous host material and a regular distribution of square scatterers. The scatterer material (Phase 2) is chosen to be stiff and heavy, and the host material (Phase 1) is compliant and light with a Young modulus ratio between both phases: $E_2/E_1 = 5$ and density ratio: $\rho_2/\rho_1 = 2$. The microcell is displayed in Figure 5a. This case is similar to the one reported in Sigmund and Søndergaard Jensen (2003).

A structured finite element mesh of 30 × 30 bilinear quadrilateral finite elements is used.

6.3.1. Discussion of results

The evaluated dispersion diagram is plotted in Figure 5b. The six bands with lower frequencies are shown. They have been obtained using 100 wavenumber points along the path Γ – X of the IFBZ perimeter, in the ***k***-space. The band structure for these wavenumbers compares very well with the ones reported in Sigmund and Søndergaard Jensen (2003).

Pictures in Figure 5c–k display, as vector fields, the shape of the modes associated with the points A_1, A_2, ..., D_1, C_2, C_3, in the band diagrams.

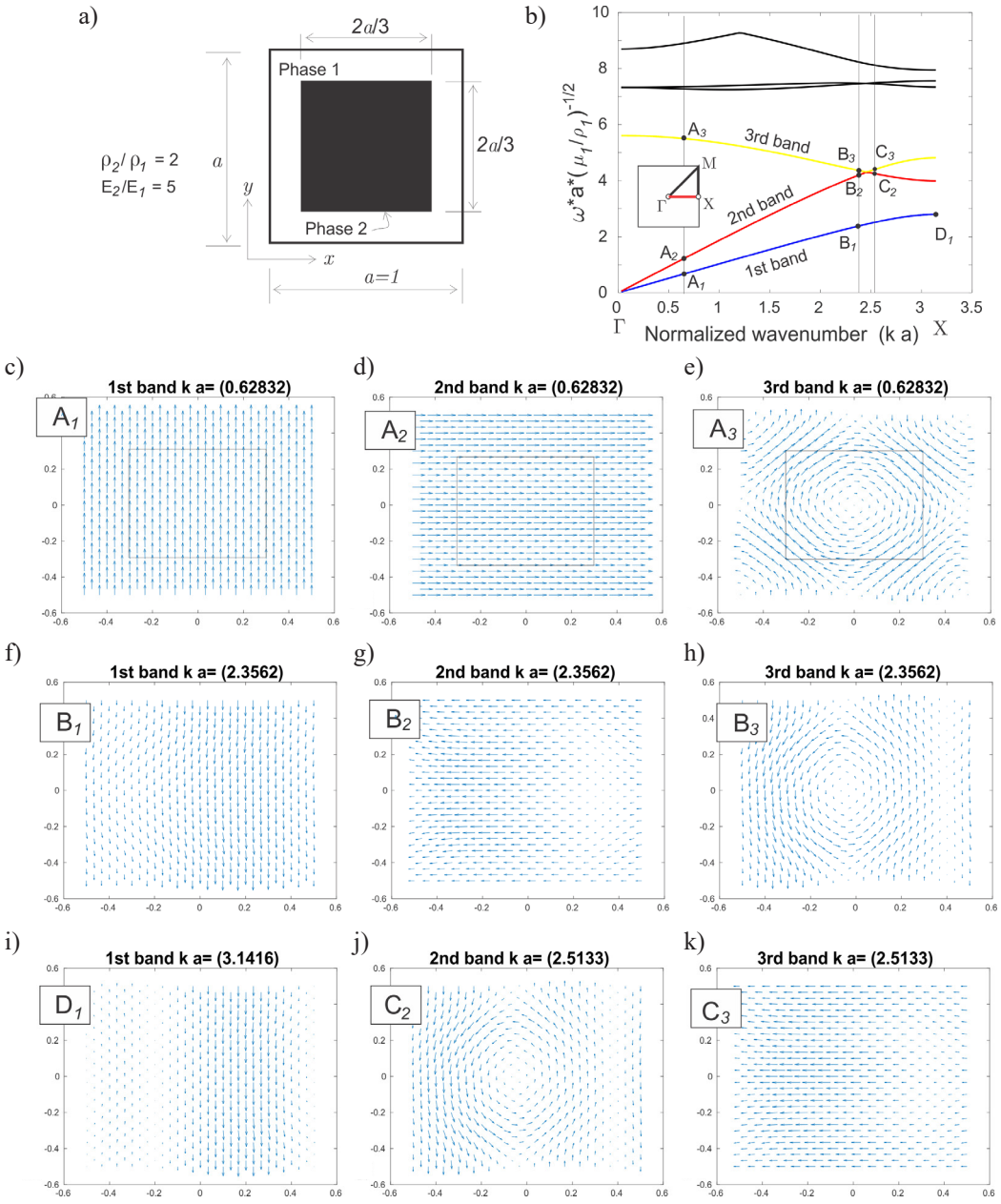

Fig. 5. Composite with square scatterers: a) microcell geometry; b) band structure for the six lower frequencies in the region Γ – X of the IFBZ; d–k) vector fields of the modes for the points A_1, A_2, ..., D_1, C_2, C_3, displayed in the band structure

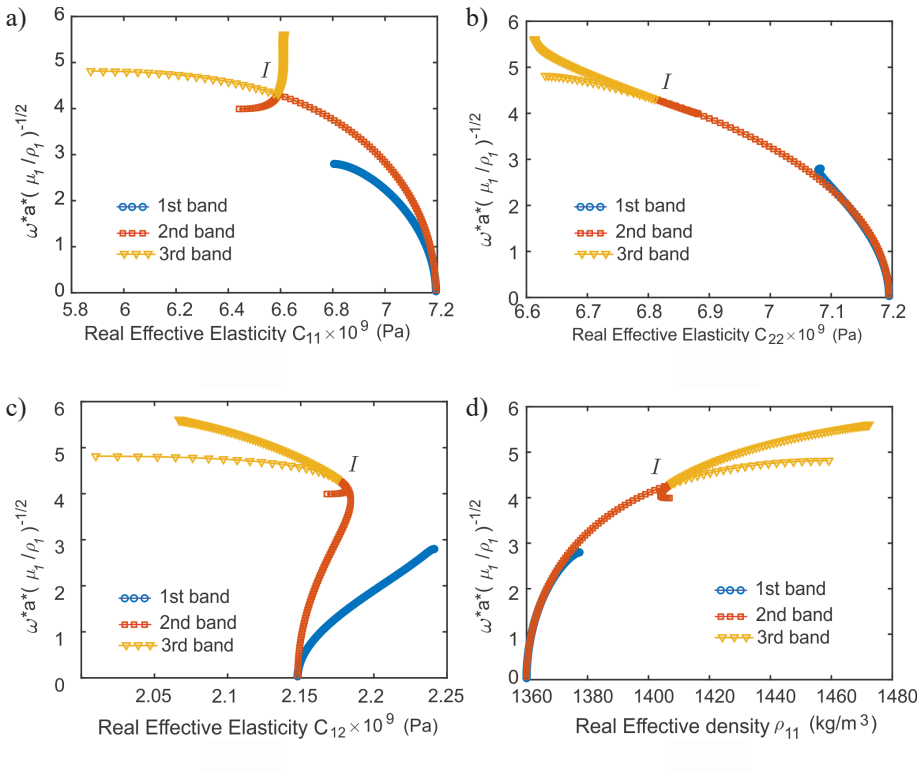

Fig. 6. Composite with square scatterers. Effective elastodynamic properties. Elasticity tensor components $\mathbb{C}^*_{11}$ (a), $\mathbb{C}^*_{22}$ (b), $\mathbb{C}^*_{12}$ (c) and effective density component $\boldsymbol{\rho}^*_{11}$ (d)

The first band is a transversal mode, the second one is a longitudinal mode, and the third band corresponds to wave propagation involving scatterer rotations. The second band intersects the third band. This characteristic can be noted in the behaviour of the effective properties at intersection point I in Figure 6.

Figure 6 plots the effective elastodynamic properties of the composites vs. angular frequency for the three bands with lower frequencies. The plots correspond to the effective elasticity tensor components $\mathbb{C}^*_{11}$, $\mathbb{C}^*_{22}$ and $\mathbb{C}^*_{12}$, respectively, defined in Equation (42) and the effective density component $\boldsymbol{\rho}^*_{11}$, defined in Equation (45).

The computational cost demanded in a laptop to perform the present evaluation (mesh 30 × 30 and 100 points in the path Γ – X) is 22 sec for computing the band structure and 1169 sec for evaluating the effective properties. The high computational cost to determine the effective properties, relative to the band structure calculation, is due to the evaluation of the inverse matrix $\mathbb{D}$ in equations (37)–(40). We note that computational cost efficiency has not been pursued in the present work.

7. Conclusions

In this paper, we have presented a homogenization model which evaluates the effective elastodynamic properties of acoustic metamaterials. The model predicts the effective properties of the constitutive equation described in terms of averaged quantities. In this sense, the approach follows very closely the original ideas introduced by Willis and posteriorly reported in the works of Nemat-Nasser and co-authors, Nassar et al., etc.

The distinctive characteristic of our approach is that we have written the microscale equations in the spatial domain with a pointwise determination of the eigenfields. A consequence of this feature is that the numerical technique for solving the equations can be directly formulated with the finite element method, if compared with the ones based on specifying the equations in the Fourier space or using integral equations to find the eigenfields. The results that we attain with this model have been contrasted with those published in the literature (Nemmat-Nasser & Srivastava, 2011). The agreement between both solutions is almost exact. Therefore, we consider that these outcomes validate the present model. Furthermore, a 2D analysis is also discussed.

The model reported in this work could be used for the topology design of acoustic metamaterials (see for example Dong et al., 2017). The evaluation of effective parameters, in addition to the dispersion curves, would be an additional ingredient that could help to determine some specific design criteria.

References

Dong, H.-W., Zhao, S.-D., Wang, Y.-S., & Zhang, C. (2017). Topology optimization of anisotropic broadband double-negative elastic metamaterials. *Journal of the Mechanics and Physics of Solids*, *105*, 54–80.

Gazalet, J., Dupont, S., Kastelik, J.C., Rolland, Q., & Djafari-Rouhani, B. (2013). A tutorial survey on waves propagating in periodic media: Electronic, photonic and phononic crystals. Perception of the Bloch theorem in both real and Fourier domains. *Wave Motion*, *50*(3), 619–654.

Hussein, M.I., Leamy, M.J., & Ruzzene, M. (2014). Dynamics of phononic materials and structures: Historical origins, recent progress, and future outlook. *Applied Mechanics Reviews*, *66*(4), 040802.

Krattiger, D., & Hussein, M.I. (2018). Generalized Bloch mode synthesis for accelerated calculation of elastic band structures. *Journal of Computational Physics*, *357*, 183–205.

Milton, G.W., & Willis, J.R. (2007). On modifications of Newton's second law and linear continuum elastodynamics. *Proceedings of the Royal Society A: Mathematical, Physical and Engineering Sciences*, *463*(2079), 855–880.

Nassar, H., He, Q.-C., & Auffray, N. (2015). Willis elastodynamic homogenization theory revisited for periodic media. *Journal of the Mechanics and Physics of Solids*, *77*, 158–178.

Nassar, H., He, Q.-C., & Auffray, N. (2016). A generalized theory of elastodynamic homogenization for periodic media. *International Journal of Solids and Structures*, *84*, 139–146.

Nemat-Nasser, S., & Srivastava, A. (2011). Overall dynamic constitutive relations of layered elastic composites. *Journal of the Mechanics and Physics of Solids*, *59*(10), 1953–1965.

Nemat-Nasser, S., Willis, J.R., Srivastava, A., & Amirkhizi, A.V. (2011). Homogenization of periodic elastic composites and locally resonant sonic materials. *Physical Review B*, *83*(10), 104103.

Roca, D., Yago, D., Cante, J., Lloberas-Valls, O., & Oliver, J. (2019). Computational design of locally resonant acoustic metamaterials. *Computer Methods in Applied Mechanics and Engineering*, *345*, 161–182.

Sigmund, O., & Søndergaard Jensen, J. (2003). Systematic design of phononic band–gap materials and structures by topology optimization. *Philosophical Transactions of the Royal Society of London. Series A: Mathematical, Physical and Engineering Sciences*, *361*(1806), 1001–1019.

Srivastava, A. (2015). Elastic metamaterials and dynamic homogenization: a review. *International Journal of Smart and Nano Materials*, *6*(1), 41–60.

Srivastava, A., & Nemat-Nasser, S. (2014). On the limit and applicability of dynamic homogenization. *Wave Motion*, *51*(7), 1045–1054.

Willis, J.R. (1997). Dynamics of composites. In P. Suquet (Ed.), *Continuum micromechanics* (pp. 265–290). Springer-Verlag Wien.

Willis, J.R. (2012). The construction of effective relations for waves in a composite. *Comptes Rendus Mécanique*, *340*(4–5), 181–192.